Inorg. Chem. **2007**, *46*, 10158–10167

Oxygen-Bridged Hybrid Metallocene–Nonmetallocene Polymetallic Catalysts of Group 4 Metals for Bimodal Activity in Olefin Polymerization: Synthesis, Characterization, and Theoretical Investigation†

Swadhin K. Mandal,‡ Prabhuodeyara M. Gurubasavaraj,‡ Herbert W. Roesky,*,‡ Gerald Schwab,‡ Dietmar Stalke,‡ Rainer B. Oswald,§ and Volker Dolle||

Institute of Inorganic Chemistry, University of Göttingen, Tammannstrasse 4, 37077 Göttingen, Germany, Institute of Physical Chemistry, University of Göttingen, Tammannstrasse 6, 37077 Göttingen, Germany, Basell R & D Polymer Physics and Characterization, Industriepark, Hoechst, Frankfurt, Germany

Received June 16, 2007

This article describes the syntheses of two covalently linked oxygen-bridged hybrid metallocene–nonmetallocene polymetallic catalysts bearing two different catalytically active group 4 metals. The reactions of $Cp^*_2(Me)Zr(OH)$ (**2**) with $Ti(NMe_2)_4$ and $Hf(NMe_2)_4$ led to the formation of a heterobimetallic compound $Cp^*_2(Me)Zr(\mu\text{-}O)Ti(NMe_2)_3$ (**7**) and a trimetallic derivative $Cp^*_2(Me)Zr(\mu\text{-}O)Hf(NMe_2)_2(\mu\text{-}O)Zr(Me)Cp^*_2$ (**9**), respectively, under the elimination of Me_2NH. The crystal data confirm the molecular structures of **7** and **9**, which crystallize in the space groups $P\bar{1}$ and $P2_1/n$, respectively. **9** is the first example of a crystallographically characterized heterotrimetallic complex having a Zr–O–Hf–O–Zr core. **7** bearing two active catalytic centers, namely, zirconium and titanium, exhibits bimodal activity in olefin polymerization when activated with methylalumoxane (MAO). It produces polyethylene largely controlled by the zirconium center, and polystyrene seems to be formed predominantly by the titanium center. DFT calculations were performed on the supposed cationic intermediates, revealing that a cation generated on the titanium center is sterically more accessible for monomer binding, though it is energetically less-favorable than that generated on the zirconium center.

Introduction

Poly- and heterometallic complexes in general have enormous potential to revolutionize homogeneous catalytic processes. They can simultaneously activate both components of a bimolecular reaction, overcome entropy barriers associated with bringing the two reagents together, and minimize the energy barrier that arises from solvent−shell rearrangements during the reaction by virtue of the cooperative interaction between the two different metal centers.[1] In this way, a very important area of tandem catalysis has burgeoned in recent years, in which one site produces a specific type of polymer that is immediately incorporated into another type of polymer produced by the other proximate metal center.[2−6] The synthesis and characterization of heterobimetallic oxides, which are used as polyfunctional catalysts and precursors for the preparation of bi- and polymetallic heterogeneous catalysts, have been the topic of various academic and industrial studies[7,8] since the discovery of the catalytic olefin polymerization by Ziegler and Natta. These heterogeneous

† Dedicated to Professor C. N. R. Rao on the occasion of his 73rd birthday.

* To whom correspondence should be addressed. E-mail: hroesky@gwdg.de.
‡ Institute of Inorganic Chemistry, University of Göttingen.
§ Institute of Physical Chemistry, University of Göttingen.
|| Basell R & D Polymer Physics and Characterization.

(1) Stephan, D. W. *Coord. Chem. Rev.* **1989**, *95*, 41−107.
(2) Alt, H. G.; Koeppl, A. *Chem. Rev.* **2000**, *100*, 1205−1221.
(3) Abramo, G. P.; Li, L.; Marks, T. J. *J. Am. Chem. Soc.* **2002**, *124*, 13966−13967.
(4) Komon, Z. J. A.; Bu, X.; Bazan, G. C. *J. Am. Chem. Soc.* **2000**, *122*, 1830−1831.
(5) Komon, Z. J. A.; Bu, X.; Bazan, G. C. *J. Am. Chem. Soc.* **2000**, *122*, 12379−12380.
(6) Komon, Z. J. A.; Diamond, G. M.; Leclerc, M. K.; Murphy, V.; Okazaki, M.; Bazan, G. C. *J. Am. Chem. Soc.* **2002**, *124*, 15280−15285.
(7) Copéret, C.; Chabanas, M.; Saint-Arroman, R. P.; Basset, J.-M. *Angew. Chem.* **2003**, *115*, 164−191. *Angew. Chem., Int. Ed.* **2003**, *42*, 156−181.
(8) Roesky, H. W.; Haiduc, I.; Hosmane, N. S. *Chem. Rev.* **2003**, *103*, 2579−2595.

10.1021/ic7011765 CCC: $37.00
Published on Web 10/24/2007

Chart 1. Some Recently Developed Active Heterobimetallic Catalysts for Polymerization

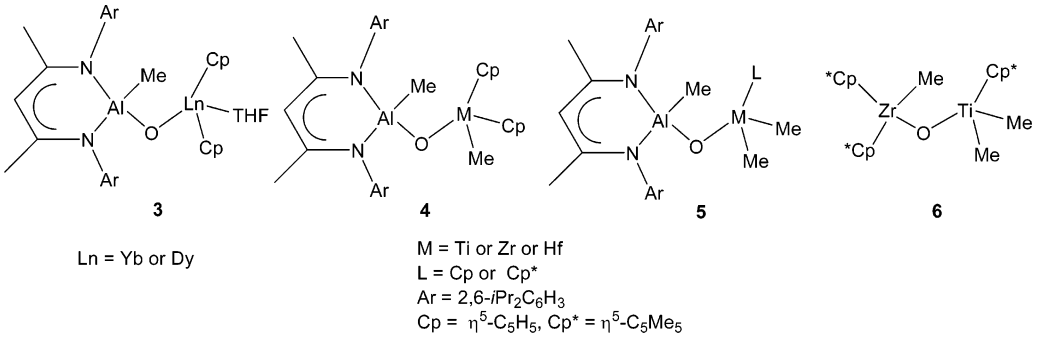

catalysts have complicated structural features and are insoluble in solvents that are advantageous for polymerization reactions. Investigations by Sinn and Kaminsky et al.[9−11] reveal that soluble metallocene catalysts in combination with methylalumoxane (MAO) achieve extremely high activities in the polymerization of olefins, leading to new developments in this field. Subsequent years have witnessed tremendous advances in the design and application of organometallic complexes as olefin polymerization catalysts; and to date, the homogeneous organometallic catalysts active for olefin polymerization can broadly be categorized into two classes: the metallocene-based catalysts[2,12−14] and the nonmetallocene-based catalysts.[15−21] However, efforts have also been made to develop MAO-free catalyst systems due to the use of a high amount of MAO, high temperature, and the poorly understood MAO-based cocatalyst system. For example, Grubbs and co-workers have developed a family of late-transition-metal catalysts based on nickel(II) salicylaldimine complexes, which are highly active systems producing high molecular weight polyethylene and polymerizing functionalized olefins in the absence of any added cocatalyst.[22] Several other naked cationic complexes developed by Jordan et al.[23] and Marks and co-workers[24] based on early transition metals such as $[Cp_2(Me)Zr(THF)]^+[BPh_4]^-$ and $[Cp_2(Me)Zr]^+[B(C_6F_5)_3(Me)]^-$ are now available and can catalyze olefin polymerization with comparable-to-better catalytic activity than the traditional metallocene/MAO-based catalysts.

We have reported the development of a new class of heterobimetallic complexes through oxygen bridging, which are excellent candidates for homogeneous catalysis,[25−28] and this topic was recently reviewed.[29] The synthetic strategy takes advantage of unprecedented syntheses of two monometallic hydroxide precursors, L(Me)Al(OH) (**1**)[25] [L = CH{N(Ar)(CMe)}$_2$, Ar = 2,6-*i*Pr$_2$C$_6$H$_3$] and Cp*$_2$(Me)Zr(OH) (**2**).[28] The Brönsted acidic character of the proton in the Al(O−H) or Zr(O−H) moiety allows building a plethora of heterobimetallic complexes of the types **3**−**6** (Chart 1) useful for polymerization catalysis.[25−28] For example, synthesis of a new class of compounds containing a Ln−O−Al moiety (**3**, Chart 1) provides a stable framework to assemble new complexes exhibiting good catalytic activity for the polymerization of ϵ-caprolactone.[26] Recently, we have reported the reactions of **1** with a variety of metallocene-based group 4 metal precursors, leading to the formation of oxygen-based heterobimetallic catalytic systems (**4**−**5**, Chart 1).[25,27] It was observed that these catalysts (**4**−**5**) are very active in ethylene polymerization at unusually low MAO concentration, and this could probably be attributed to the presence of a chemically grafted (Me)Al−O backbone in the catalysts, a part of externally added cocatalyst MAO. Also, the bridging oxygen might play an important role in determining the Lewis acidity at the active metal center. Recently, **6** was prepared by reacting Cp*$_2$(Me)Zr(OH) (**2**) with Cp*TiMe$_3$ under the elimination of methane. This is the first example of an oxygen-bridged heterobimetallic catalyst bearing two different active group 4 metal centers exhibiting very high catalytic activity in ethylene polymerization.[28]

Herein, we report the synthesis, characterization, and theoretical investigation of a new class of oxygen-bridged

(9) Andresen, A.; Cordes, H.-G.; Herwig, J.; Kaminsky, W.; Merck, A.; Mottweiler, R.; Pein, J.; Sinn, H.; Vollmer, H.-J. *Angew. Chem.* **1976**, *88*, 689−690. *Angew. Chem., Int. Ed. Engl.* **1976**, *15*, 630−632.
(10) Sinn, H.; Kaminsky, W.; Vollmer, H.-J.; Woldt, R. *Angew. Chem.* **1980**, *92*, 396−402. *Angew. Chem., Int. Ed. Engl.* **1980**, *19*, 390−392.
(11) Sinn, H.; Kaminsky, W. *Adv. Organomet. Chem.* **1980**, *18*, 99−149.
(12) Brintzinger, H. H.; Fischer, D.; Mülhaupt, R.; Rieger, B.; Waymouth, R. M. *Angew. Chem.* **1995**, *107*, 1255−1283. *Angew. Chem., Int. Ed. Engl.* **1995**, *34*, 1143−1170.
(13) Jordan, R. F. *Adv. Organomet. Chem.* **1991**, *32*, 325−387.
(14) McKnight, A. L.; Waymouth, R. M. *Chem. Rev.* **1998**, *98*, 2587−2598.
(15) Britovsek, G. J. P.; Gibson, V. C.; Wass, D. F. *Angew. Chem.* **1999** *111*, 448−468. *Angew. Chem., Int. Ed.* **1999**, *38*, 428−447.
(16) Mason, A. F.; Coates, G. W. *J. Am. Chem. Soc.* **2004**, *126*, 16326−16327.
(17) Reinartz, S.; Mason, A. F.; Lobkovsky, E. B.; Coates, G. W. *Organometallics* **2003**, *22*, 2542−2544.
(18) Zhang, L.; Brookhart, M.; White, P. S. *Organometallics* **2006**, *25*, 1868−1874.
(19) Stapleton, R. L.; Chai, J.; Taylor, N. J.; Collins, S. *Organometallics* **2006**, *25*, 2514−2524.
(20) Gottfried, A. C.; Brookhart, M. *Macromolecules* **2003**, *36*, 3085−3100.
(21) Stapleton, R. A.; Chai, J.; Nuanthanom, A.; Flisak, Z.; Nele, M.; Ziegler, T.; Rinaldi, P. L.; Soares, J. B. P.; Collins, S. *Macromolecules* **2007**, *40*, 2993−3004.
(22) Younkin, T. R.; Connor, E. F.; Henderson, J. I.; Friedrich, S. K.; Grubbs, R. H.; Bansleben, D. A. *Science* **2000**, *287*, 460−462.
(23) Jordan, R. F.; Bajgur, C. S.; Willet, R.; Scot, B. *J. Am. Chem. Soc.* **1986**, *108*, 7410.
(24) Yang, X.; Stern, C. L.; Marks, T. J. *J. Am. Chem. Soc.* **1991**, *113*, 3623−3625.
(25) Bai, G.; Singh, S.; Roesky, H. W.; Noltemeyer, M.; Schmidt, H.-G. *J. Am. Chem. Soc.* **2005**, *127*, 3449−3455.
(26) Chai, J.; Jancik, V.; Singh, S.; Zhu, H.; He, C.; Roesky, H. W.; Schmidt, H.-G.; Noltemeyer, M.; Hosmane, N. S. *J. Am. Chem. Soc.* **2005**, *127*, 7521−7528.
(27) Gurubasavaraj, P. M.; Mandal, S. K.; Roesky, H. W.; Oswald, R. B.; Pal, A.; Noltemeyer, M. *Inorg. Chem.* **2007**, *46*, 1056−1061.
(28) Gurubasavaraj, P. M.; Roesky, H. W.; Sharma, P. M. V.; Oswald, R. B.; Dolle, D.; Pal, A. *Organometallics* **2007**, *26*, 3346−3351.
(29) Singh, S.; Roesky, H. W. *Dalton Trans.* **2007**, 1360−1370.

Scheme 1

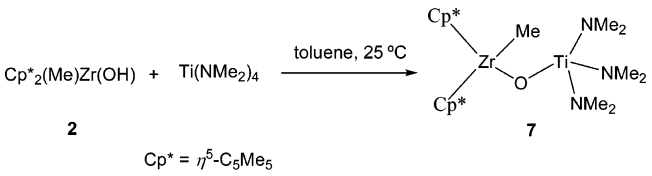

hybrid metallocene−nonmetallocene compounds consisting of two different active catalytic centers of group 4 metals. One of these compounds, $Cp^*_2(Me)Zr(\mu\text{-}O)Ti(NMe_2)_3$ (**7**) bearing two active catalytic centers, namely, zirconium and titanium, exhibits bimodal activity in olefin polymerization when activated with MAO. It produces polyethylene largely by the zirconium center and also polymerizes styrene predominantly by the titanium center. DFT calculations were performed on the supposed cationic intermediates, to understand the catalytic process.

Results and Discussion

Syntheses and Reactivity of Oxygen Bridged Metallocene−Nonmetallocene Hybrid Polymetallic Catalysts. Synthesis of $Cp^*_2(Me)Zr(\mu\text{-}O)Ti(NMe_2)_3$ (**7**) containing the Zr−O−Ti motif (Scheme 1) was accomplished by reacting the monometallic hydroxide precursor, $Cp^*_2(Me)Zr(OH)$ (**2**)[28] with $Ti(NMe_2)_4$ under the elimination of Me_2NH in high yield. The solution of $Cp^*_2(Me)Zr(OH)$ in toluene was added drop-by-drop to the solution of $Ti(NMe_2)_4$ in a 1:1 stoichiometric ratio in toluene and stirred at 25 °C for 14 h to yield the yellow complex, **7**. The ^{1}H NMR spectrum of the reaction mixture reveals almost quantitative conversion of the reactants to product, as revealed by the absence of any characteristic Zr−OH resonance at 4.2 ppm in C_6D_6. **7** is insoluble in *n*-hexane or pentane but readily soluble in toluene and benzene at room temperature. **7** was characterized by ^{1}H and ^{13}C NMR spectroscopy, analytical data, EI mass spectrometry, and single-crystal X-ray diffraction studies. The ^{1}H NMR spectrum of **7** in C_6D_6 exhibits three singlets (0.01, 1.89, and 3.14 ppm) attributed to the proton resonances arising from Zr−Me, η^5-C_5Me_5, and NMe_2 groups, respectively. The singlet at 0.01 ppm integrates one-sixth against the singlet at 3.14 ppm, revealing the formation of a bimetallic **7**, as formulated in Scheme 1. The ^{13}C NMR spectrum of **7** reveals a resonance at 29.1 ppm, assigned to the zirconium-bound methyl-carbon resonance. The six methyl-carbon nuclei arising from the three dimethylamino groups attached to the titanium center resonate at 45.4 ppm. Additionally, the resonaces at 11.3 and 117.7 ppm are assigned to the carbon atoms of the methyl groups and η^5-cyclopentadienyl from the zirconium-bound Zr−C_5Me_5 groups, respectively. Analytically pure crystals of **7** were obtained from cold toluene at −20 °C, and finally the structure of **7** was unambiguously determined by single-crystal X-ray crystallography (below).

7 breaks up to monohydroxide **2**, and an unidentified product, when exposed to moisture, as revealed by the characteristic Zr−OH resonance in the ^{1}H NMR spectrum (4.2 ppm in C_6D_6). The reaction of **7** with Me_2SiCl_2 leads to the cleavage of the Zr−O−Ti bond and a chlorine transfer reaction, forming $Cp^*_2ZrCl_2$ and other unidentified products (Scheme 2). However, **7** was found to be remarkably stable for several months under an inert atmosphere. Further reaction of **7** with 1 equiv of $Cp^*_2(Me)Zr(OH)$ (**2**) in toluene does not lead to the formation of the expected heterotrimetallic complex bearing the Zr−O−Ti−O−Zr moiety. **7** does not undergo further reaction with **2** to form a heterotrimetallic complex that can probably be attributed to the steric demand imposed by the bulky Cp* ligands of **2**, hindering further transformation of **7** into a trimetallic complex.

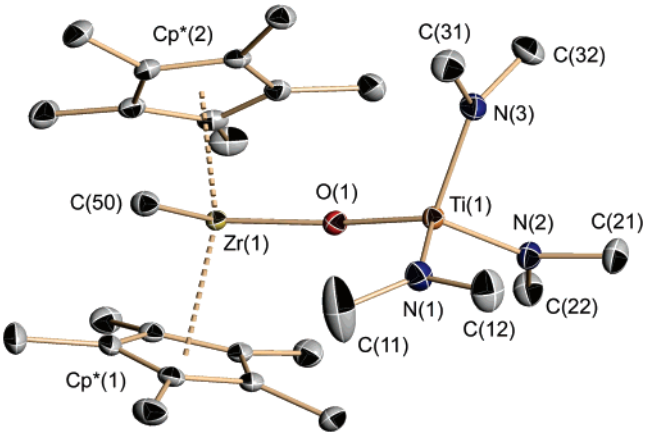

Figure 1. Molecular structure of **7** in the crystal (50% probability ellipsoids); hydrogen atoms are omitted for clarity.

However, $Hf(NMe_2)_4$ reacts in a different way with $Cp^*_2(Me)Zr(OH)$ (**2**) than $Ti(NMe_2)_4$. The solution of $Cp^*_2(Me)Zr(OH)$ in toluene was added drop-by-drop to the solution of $Hf(NMe_2)_4$ in a 1:1 stoichiometric ratio in toluene and stirred at 25 °C for 24 h to yield a colorless heterobimetallic compound $Cp^*_2(Me)Zr(\mu\text{-}O)Hf(NMe_2)_3$ (**8**) along with another minor product in a 4:1 molar ratio. **8** could not be isolated in a pure form, but it was formulated as a heterobimetallic complex shown in Scheme 3 by its characteristic ^{1}H NMR pattern. The ^{1}H NMR spectrum of **8** reveals a 1:6 relative intensity ratio of Zr−Me to NMe_2 protons, indicating a heterobimetallic formulation of **8**. The structure of the minor compound was established as the heterotrimetallic $Cp^*_2(Me)Zr(\mu\text{-}O)Hf(NMe_2)_2(\mu\text{-}O)Zr(Me)Cp^*_2$ (**9**) complex. This compound was prepared in higher yield using different stoichiometry of the reactants. A toluene solution of $Cp^*_2(Me)Zr(OH)$ was added to the solution of $Hf(NMe_2)_4$ in toluene in a 2:1 stoichiometric ratio and stirred at 25 °C for 24 h, yielding almost quantitatively the heterotrimetallic complex **9**, as revealed by the ^{1}H NMR spectrum of the reaction mixture. **9** is soluble in toluene and benzene at room temperature. **9** was characterized by ^{1}H and ^{13}C NMR spectroscopy, analytical data, EI mass spectrometry, and single-crystal X-ray diffraction studies. Analytically pure crystals of **9** were obtained from cold toluene at −20 °C. The ^{1}H NMR spectrum of **9** exhibits three singlets (−0.05, 1.92, and 2.99 ppm) assigned to the proton resonances arising from Zr−Me, the η^5-C_5Me_5 ligands, and two NMe_2 groups, respectively. The singlet at 2.99 ppm integrates twice against the singlet at −0.05 ppm, clearly suggesting the formation of trimetallic **9**, as formulated in Scheme 3. The ^{13}C NMR spectrum is almost similar to that observed

Scheme 2

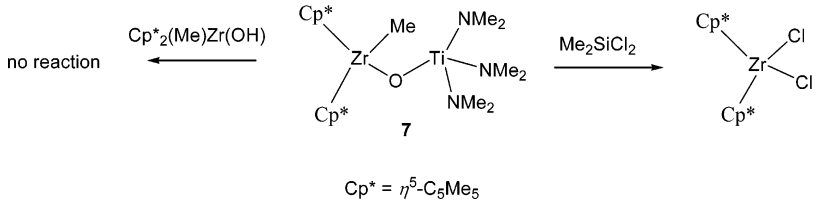

Scheme 3

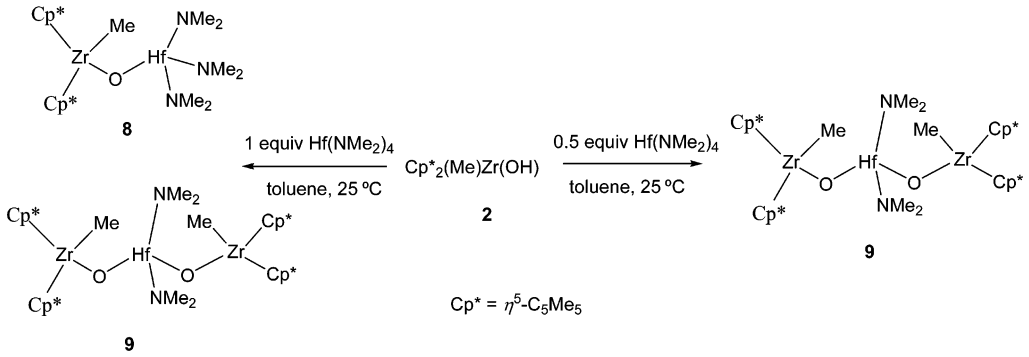

for heterobimetallic **7**, exhibiting singlets at 27.9 and 43.5 ppm assigned to the carbon resonances arising from Zr−Me and Hf−NMe_2 groups, respectively.

The EI mass spectral data for both **7** and **9** are in accord with the assigned structures. Neither of them exhibits a molecular ion. **7** shows a peak at *m*/*e* 556.2 corresponding to $[M - Me]^+$. The next fragment for **7** is observed at *m*/*e* 526.2 corresponding to $[M - NMe_2]^+$. **9** exhibits an ion at *m*/*e* 1037.3 corresponding to $[M - Me]^+$.

X-ray Crystal Structures of 7 and 9. Suitable crystals for X-ray structural analysis were obtained by cooling a toluene solution of **7** at −20 °C for several days. **7** crystallizes in the triclinic space group $P\bar{1}$. The molecular structure of **7** is shown in Figure 1. The zirconium and titanium centers in **7** adopt distorted-tetrahedral geometry. The coordination sphere of the zirconium center consists of two Cp* ligands, one methyl group, and one (μ-O) unit, whereas that of the titanium has three dimethylamino groups and one (μ-O) unit. Table 1 lists crystallographic data, and Table 2 compiles the selected bond distances and angles for **7**. The bonding parameters compare well with the related oxygen-bridged heterobimetallic complex, $Cp^*_2(Me)Zr(\mu\text{-}O)Ti(Me)_2Cp^*$ (**6**).[28] **7** exhibits a slightly bent Zr−O−Ti core. The Zr(1)−O(1)−Ti(1) bond angle in **7** is 169.73(6)°, which is considerably wider than the Zr−O−Ti bond angle (156.1(2)°) observed in $Cp^*_2(Me)Zr(\mu\text{-}O)Ti(Me)_2Cp^*$ (**6**) but comparable to the homobimetallic M−O−M (M = Zr, Ti) angles in compounds $\{Cp_2Zr(Me)\}_2(\mu\text{-}O)$ (174.1(3)°)[30] and $\{Cp_2Ti(CF_3C{=}C(H)CF_3)\}_2(\mu\text{-}O)$ (170.0(2)°).[31] The Zr−C(50) bond distance (2.2950(15) Å) is comparable to the average Zr−C bond length in $Cp_2Zr(CH_2SiMe_3)_2$ (average 2.284 Å) but is slightly longer than the value (average 2.251 Å) found for $(\eta^5\text{-}C_9H_7)_2Zr(Me)_2$.[30] The Zr(1)−O(1) (2.0016-(10) Å) bond distance is comparable to the Zr−O bond distance (2.022(4) Å) observed in $Cp^*_2(Me)Zr(\mu\text{-}O)Ti(Me)_2Cp^*$ (**6**) but shorter than the heterobimetallic alkoxide-bridged clusters $Ti_4Zr_4O_6(OBu)_4(OMc)_{16}$ (OMc = methacrylate, average Zr−O 2.17 Å).[32] The angle between the centroids of Cp* and the Zr center (136.0°) is slightly wider when compared with that of $Cp^*_2(Me)Zr(\mu\text{-}O)Ti(Me)_2Cp^*$ (134.1°).

Table 1. Crystallographic Data and Structure Refinement for **7** and **9**

compound	**7**	**9**
empirical formula	$C_{27}H_{51}N_3OTiZr$	$C_{46}H_{78}Hf\,N_2O_2Zr_2$
CCDC number	642715	642716
fw	572.83	1052.03
T (K)	100(2)	100(2)
cryst size (mm^3)	0.25 × 0.20 × 0.10	0.4 × 0.2 × 0.15
space group	$P\bar{1}$	$P2_1/n$
a (Å)	10.6644(5)	14.8318(8)
b (Å)	11.6310(5)	18.7743(10)
c (Å)	12.9048(6)	17.7562(9)
α (deg)	89.4060(10)	90
β (deg)	89.3900(10)	111.0510(10)
γ (deg)	66.0210(10)	90
V (nm^3)	1.46242(12)	4.6144(4)
Z	2	4
μ_{calcd} (mm^{-1})	0.651	2.724
F (000)	608	2144
2θ range (deg)	4.18−52.78	3.08−52.74
no. of coll. reflns.	26 990	76 389
no. of indep. reflns.	5981	9408
data / restns / params	5981 / 0 / 315	9408 / 0 / 478
GOF	1.088	1.037
R1, wR2 [$I > 2\sigma(I)$][a,b]	0.0226, 0.0630	0.0220, 0.0606
R1, wR2 (all data)	0.0241, 0.0637	0.0234, 0.0613
g_1, g_2[c]	0.0368, 0.4719	0.0312, 10.4730
largest diff peak/hole (e $Å^{-3}$)	0.609 / −0.503	0.821 / −0.705

[a] $R1 = \sum||F_o| - |F_c||/\sum|F_o|$. [b] $wR2 = [\sum w(F_o^2 - F_c^2)^2/\sum w(F_o^2)^2]^{0.5}$. [c] $w = [\sigma^2(F_o^2) + (g_1P)^2 + g_2P]^{-1}$, $P = {}^1/_3[\max(F_o^2,0) + 2F_c^2]$.

Colorless crystals of **9** suitable for X-ray structural analysis were obtained from toluene at −20 °C. **9** crystallizes in the monoclinic space group $P2_1/n$. The molecular structure is

(30) Hunter, W. E.; Hrncir, D. C.; Bynum, R. V.; Penttila, R. A.; Atwood, J. L. *Organometallics* **1983**, *2*, 750−755.
(31) Rausch, M. D.; Sikora, D. J.; Hrncir, D. C.; Hunter, W. E.; Atwood, J. L. *Inorg. Chem.* **1980**, *19*, 3817−3821.
(32) Moraru, B.; Kickelbick, G.; Schubert, U. *Eur. J. Inorg. Chem.* **2001**, 1295−1301.

Table 2. Selected Bond Distances (Angstroms) and Angles (Degrees) for **7** and **9**

7			
Ti(1)−O(1)	1.8028(10)	Ti(1)−N(1)	1.9088(14)
Ti(1)−N(2)	1.9129(13)	Ti(1)−N(3)	1.9316(13)
Zr(1)−O(1)	2.0016(10)	Zr(1)−C(50)	2.2950(15)
Cp*(1)−Zr(1)[a]	2.278(8)	Cp*(2)−Zr(1)[a]	2.263(7)
O(1)−Ti(1)−N(1)	109.73(5)	O(1)−Ti(1)−N(2)	111.19(5)
N(1)−Ti(1)−N(2)	114.82(6)	O(1)−Ti(1)−N(3)	118.21(5)
N(1)−Ti(1)−N(3)	101.44(6)	N(2)−Ti(1)−N(3)	101.16(6)
Ti(1)−O(1)−Zr(1)	169.73(6)	O(1)−Zr(1)−C(50)	96.92(5)
Cp*(1)−Zr(1)− Cp*(2)[a]	136.0(3)	Cp*(1)−Zr(1)−C(50)[a]	103.2(2)
Cp*(2)−Zr(1)−C(50)[a]	102.3(2)	Cp*(1)−Zr(1)−O(1)[a]	106.0(2)
Cp*(2)−Zr(1)−O(1)[a]	105.8(2)		
9			
Hf(1)−O(1)	1.9265(18)	Hf(1)−O(2)	1.9660(18)
Hf(1)−N(1)	2.042(2)	Hf(1)−N(2)	2.040(2)
Zr(1)−O(1)	1.9992(18)	Zr(1)−C(21)	2.292(3)
Cp*(1)−Zr(1)[a]	2.274(9)	Cp*(2)−Zr(1)[a]	2.279(9)
Zr(2)−O(2)	1.9754(18)	Zr(2)−C(42)	2.302(3)
Cp*(3)−Zr(2)[a]	2.287(9)	Cp*(4)−Zr(2)[a]	2.282(9)
O(1)−Hf(1)−N(1)	108.42(9)	O(1)−Hf(1)−N(2)	108.81(9)
O(1)−Hf(1)−O(2)	111.39(8)	N(1)−Hf(1)−N(2)	107.94(10)
O(2)−Hf(1)−N(1)	109.64(9)	O(2)−Hf(1)−N(2)	110.55(9)
Hf(1)−O(1)−Zr(1)	169.38(10)	Hf(1)−O(2)−Zr(2)	151.25(11)
O(1)−Zr(1)−C(21)	95.28(9)	Cp*(1)−Zr(1)−Cp*(2)[a]	134.9(3)
Cp*(1)−Zr(1)−C(21)[a]	102.7(3)	Cp*(2)−Zr(1)−C(21)[a]	102.9(3)
Cp*(1)−Zr(1)−O(1)[a]	106.1(2)	Cp*(2)−Zr(1)−O(1)[a]	107.8(2)
O(2)−Zr(2)−C(42)	94.08(10)	Cp*(3)−Zr(2)− Cp*(4)[a]	134.7(3)
Cp*(3)−Zr(2)−C(42)[a]	102.4(3)	Cp*(4)−Zr(2)−C(42)[a]	102.5(3)
Cp*(3)−Zr(2)−O(2)[a]	107.8(3)	Cp*(4)−Zr(2)−O(2)[a]	107.4(2)

[a] Cp* = Centroid of the Cp* ring.

shown in Figure 2. It shows that the hafnium atom is bonded through two bridging oxygen atoms to two zirconium centers, establishing a trimetallic core with a Zr−O−Hf−O−Zr backbone. The hafnium atom exhibits a distorted-tetrahedral geometry with two nitrogen atoms of two dimethylamino ligands, and two (μ-O) units. Each zirconium center is bonded to two Cp* groups and to two ancillary ligands (Me and (μ-O)), adopting a distorted-tetrahedral geometry around the metal (Figure 2). The enhanced metal−oxygen bond distances in **9** as compared to that in **7** clearly (Table 2) indicate that the formation of the trimetallic core in the case of **9** is favored as the bulky $Cp^*_2Zr(\mu\text{-O})$ core moves further away from the central metal (Figure S1 in the Supporting Information). The other bond distances and angles involving the zirconium center in **9** compare well with those observed in **7**. **9** exhibits two different types of bent Zr−O−Hf cores. The Zr(1)−O(1)−Hf(1) bond angle in **9** is 169.38(10)°, which is similar to the observed Zr(1)−O(1)−Ti(1) bond angle (169.73(6)°) in **7**. The other Zr(2)−O(2)−Hf(1) bond angle in **9** is 151.25(11)°, which is considerably bent, and probably this bending can be attributed to the internal requirement for the formation of a trimetallic core, putting the three metal centers in an optimum steric environment.

Polymerization of Ethylene. **7** catalyzes the polymerization of ethylene in toluene, when activated with MAO. All of the polymeric materials were isolated as white powders. Table 3 represents the results of ethylene polymerization data. Figure 3 exhibits a graph of activity against the MAO-to-catalyst ratio of **7**, revealing that the highest activity is achieved at a 400:1 MAO-to-catalyst ratio. The polymerization data exhibits that **7** is a quite-active catalyst at a moderately low MAO-to-catalyst ratio.

DSC measurements show that the melting points (T_m) of the polyethylene produced by **7** are in the range of 125−129 °C. The ^{13}C NMR data exhibits a singlet at 30.0 ppm corresponding to the backbone carbon of a linear polyethylene chain. We assume that during polymerization a cleavage of the Zr−O bond occurs, leading to two single-site catalysts with oxygen bonding to the titanium species. In the present case, the polyethylene seems to be produced largely by the zirconium center, as revealed by the control experiments carried out with $Cp^*_2Zr(Me)_2$ and $Ti(NMe_2)_4$ as catalysts. $Cp^*_2Zr(Me)_2$ exhibits less-but-comparable activity in ethylene polymerization, and $Ti(NMe_2)_4$ reveals almost two orders lower activity in magnitude for ethylene polymerization, when compared to the activity observed for **7** under identical conditions (Table S1, Supporting Information). This fact was further supported by the catalytic activity observed for **9**, which shows activity higher of one order in magnitude than $Hf(NMe_2)_4$ under identical polymerization conditions, indicating that the ethylene polymerization is controlled by the zirconium center. Also, the molecular weight and monomodal polydispersities (Table 3) are consistent with single-site processes during the ethylene polymerization. The difference in the activity of the control experiments and **7** might be due to the oxygen incorporated within the titanium species. This is in accordance with other oxygen containing catalysts.[25,27−28]

Styrene Polymerization Studies. The catalytic property of **7** for the polymerization of styrene was preliminarily investigated. This complex shows moderate activity at ambient temperature in toluene when activated with MAO. All of the polymeric materials were isolated as white amorphous powders, and Table 4 summarizes the activity values of catalyst **7**, which increase gradually with the MAO-to-catalyst ratio (Figure 4). The polystyrene is most likely to be produced by the titanium center, as revealed by the control experiments carried out with $Ti(NMe_2)_4$ as catalysts exhibiting comparable activity in styrene polymerization when compared to the activity observed for **7** under identical conditions. The DSC measurements of the polystyrene obtained show that the characteristic glass-transition temperatures (T_g) are in the range from 72 to 76 °C. Melting points (T_m) for the polymers were not observed. This unusually low T_g might be attributed to the branching in the atactic polystyrenes.

Results of Computational Studies on Complex 7. It is generally accepted that the catalytically active species in olefin polymerization is a coordinatively unsaturated cationic species. To understand the catalytic process we have carried out ab initio calculations on **7**. As shown in Table 5, the calculated equilibrium structure matches very well with the data obtained by X-ray diffraction, thus giving a solid foundation for the electronic structure calculations for obtaining further insight by investigating the molecular orbitals and bonds.

The molecular orbital picture for the highest occupied molecular orbital (HOMO) and the lowest unoccupied molecular orbital (LUMO) clearly reveals that the two metallic centers are quite different in terms of the distribution

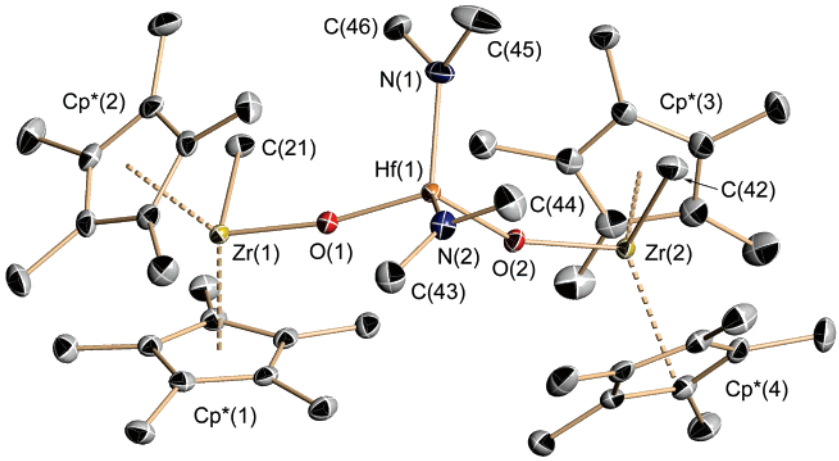

Figure 2. Molecular structure of **9** in the crystal (50% probability ellipsoids); hydrogen atoms are omitted for clarity.

Table 3. Ethylene Polymerization Data[a]

catalyst	MAO:catalyst	*PE* (g)	*A* ($\times 10^5$)	M_w	M_w/M_n	T_m[b] (°C)
7	200	0.23	0.46	(−)[c]	(−)[c]	125.9
7	300	0.25	0.50	(−)[c]	(−)[c]	126.1
7	400	0.91	1.82	170000	2.87	125.2
7	600	0.93	1.86	127000	2.74	127.1
9	400	0.47	0.94	205000	2.71	128.7

[a] Polymerization condition; 10 μmol catalyst, 100 mL of toluene at 25 °C, at 1 atm ethylene pressure for 0.5 h. Activity (*A*) = *gPE*/mol cat·h. [b] DSC. [c] Not measured.

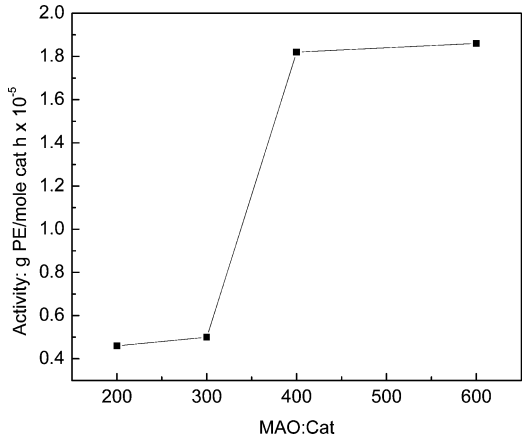

Figure 3. Plot of activity against MAO-to-catalyst ratios of **7** in ethylene polymerization.

Table 4. Styrene Polymerization Data for **7** as Catalyst[a]

catalyst	MAO:catalyst	*PS* (g)	*A* ($\times 10^4$)	T_g[b] (°C)
7	800	0.44	4.4	75.3
7	1000	0.55	5.5	70.2
7	1200	0.61	6.1	74.8
7	1600	0.84	8.4	72.0

[a] Polymerization condition; 10 μmol catalyst, 100 mL of toluene with 10 mL of styrene at 25 °C, for 1 h. Activity (*A*) = *gPS*/mol cat·h. [b] DSC.

of electron density (Figures 5 and 6). The most-striking difference can be observed by comparing the corresponding HOMO and LUMO of the cationic intermediates generated on the titanium center and on the zirconium center, respectively. The HOMO of the cation generated on the zirconium center lacks electron density as compared to that on the titanium center (parts b and c of Figure 5). On the other hand, the LUMO on the zirconium-centered cation is sterically crowded, owing to the presence of two bulky Cp* ligands in the vicinity of the zirconium center, forcing it to extend into the gap between the two Cp* ligands (part b of Figure 6), whereas the LUMO on the titanium-centered cation does not have such a steric crowding (part c of Figure 6). Additionally, the thermodynamic data unravels that the formation of the zirconium-centered cation or the titanium-centered cation is feasible energetically; however, the energy difference between the neutral compound and the titanium-centered cation is 3.5 times higher than that with the zirconium-centered cation (Figure 7). Thus, it seems reasonable to think that in the polymerization process the zirconium-centered cation being energetically more favorable predominantly takes control on the ethylene polymerization performed at a relatively lower MAO-to-catalyst ratio, and the titanium-centered cation being sterically favored predominantly takes control on the styrene polymerization performed at a relatively higher MAO-to-catalyst ratio.

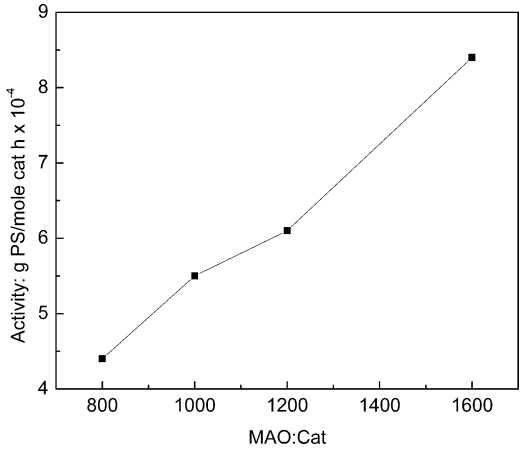

Figure 4. Plot of activity against MAO-to-catalyst ratios of **7** in styrene polymerization.

Table 5. Selected Calculated and X-ray Bond Distances (Angstroms) and Bond Angles (Degrees) of **7**

bond distances	Calcd	X−ray	bond angles	Calcd	X−ray
Zr(1)−O(1)	2.019	2.002	O(1)−Ti(1)−N(1)	110.83	109.73
Ti(1)−O(1)	1.816	1.803	N(1)−Ti(1)−N(2)	112.16	114.82
Zr(1)−C(50)	2.286	2.295	Ti(1)−O(1)−Zr(1)	171.03	169.73
Ti(1)−N(2)	1.912	1.913	O(1)−Zr(1)−C(50)	95.40	96.92

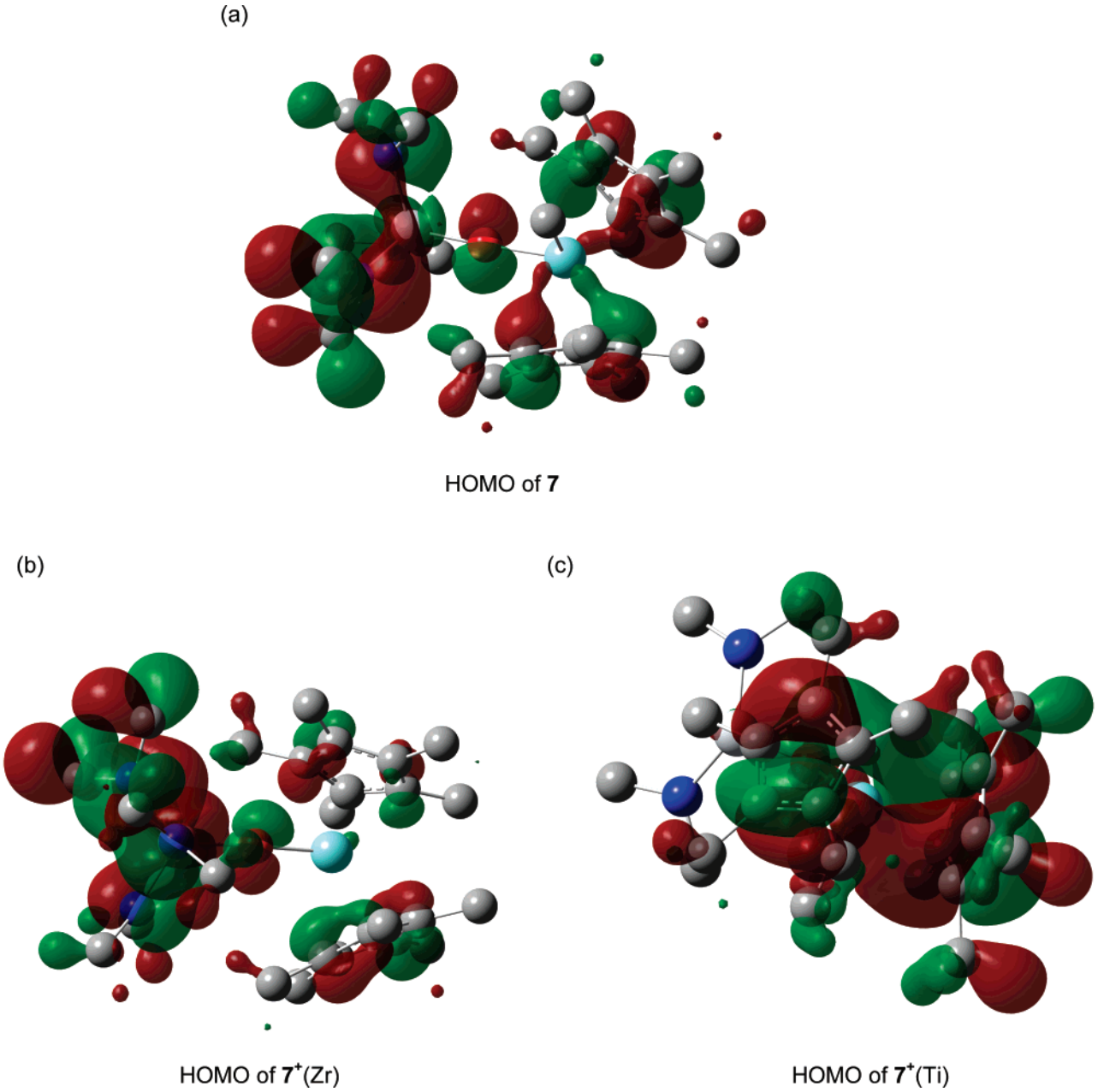

Figure 5. Computed molecular orbital picture of HOMO in **7**; (a) neutral molecule **7**, (b) zirconium-centered cation [$\mathbf{7}^{+}$(Zr)], and (c) titanium-centered cation [$\mathbf{7}^{+}$(Ti)].

Moreover, the NBO analysis shows that the Ti−O bond in the neutral molecule is composed of a $sp^{0.18}d^{2.50}$-hybrid orbital on titanium and a sp-hybrid orbital on oxygen, which transforms into $sp^{0.36}d^{66}$ and $sp^{6.48}$ in the titanium-centered cation, increasing significantly the d character on the titanium center and the p character on the oxygen center, respectively. The formation of the titanium-centered cation was stabilized by a donor−acceptor type interaction between the Ti−O bonding orbital with the lone pairs on zirconium as well as with the antibonding Zr−Cp* orbitals stabilizing 14 and 15 kcal/mol in energy, respectively.

Summary and Conclusion

In this contribution, we report a route to synthesize the hybrid metallocene−nonmetallocene catalysts bearing more than one active catalytic center through oxygen bridging and demonstrated that the two different catalytic centers can be used for bimodal activity in olefin polymerization. The synthetic strategy takes advantage of the recently synthesized kinetically stable Cp^*_2(Me)Zr(OH) (**2**) precursor as the building block and the Brönsted acidic character of the proton in the Zr(O−H) moiety, which allow us to build up the hybrid metallocene−nonmetallocene catalysts starting from bi- to trimetallic cores, by carefully changing the reaction stoichiometry as well as the nonmetallocene precursor. The heterobimetallic Zr−O−Ti complex (**7**) exhibits moderately high activity in ethylene and styrene polymerization. It produces polyethylene largely controlled by the zirconium center, and polystyrene seems to be formed predominantly by the titanium center. DFT calculations were performed on

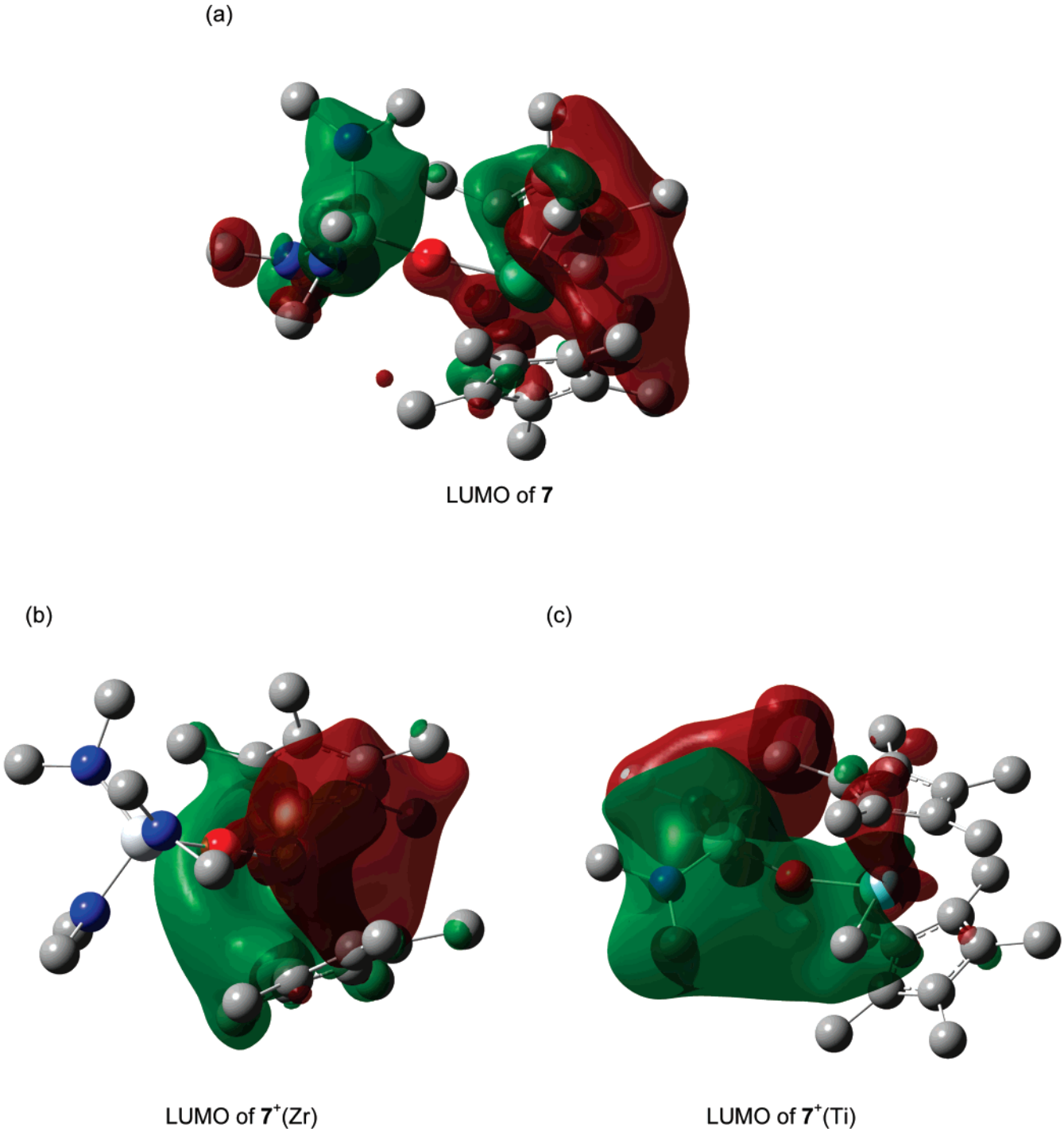

Figure 6. Computed molecular orbital picture of LUMO in **7**; (a) neutral molecule **7**, (b) zirconium-centered cation [$\mathbf{7}^+$(Zr)], and (c) titanium-centered cation [$\mathbf{7}^+$(Ti)].

the supposed cationic intermediates to understand the catalytic process. The calculations reveal that a cation generated on titanium is sterically more accessible for monomer binding, though it is energetically less favorable than that generated on the zirconium center.

Experimental Section

General Comments. All of the experimental manipulations were carried out under an atmosphere of dry argon using standard Schlenk techniques. The samples for spectral measurements were prepared in a glovebox. The solvents were purified according to conventional procedures and were freshly distilled prior to use. $Ti(NMe_2)_4$ and $Hf(NMe_2)_4$ were purchased from Alfa Aeser and used without further purification. $Cp^*_2(Me)Zr(OH)$ was prepared following the literature procedure.[28] NMR spectra were recorded on Bruker Avance 500 and Bruker Avance 300 instruments, and the chemical shifts downfield from the reference standard tetramethylsilane (TMS) were assigned positive values. Mass spectra were obtained on a Finnigan MAT 8230 spectrometer by the EI technique. Melting points were obtained in sealed capillaries on a Büchi B 540

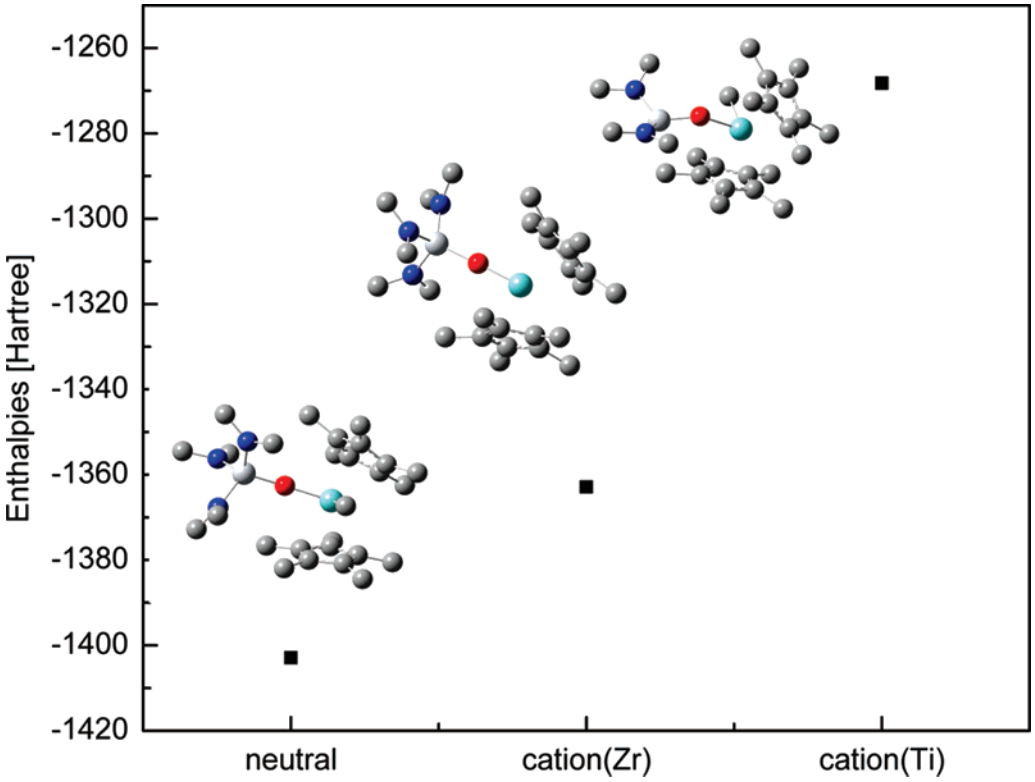

Figure 7. Enthalpy differences between the neutral molecule **7** and corresponding cationic species revealing that a cation on the titanium center is energetically less favorable than that on the zirconium center.

instrument. Elemental analyses were performed at the Analytical Laboratory of the Institute of Inorganic Chemistry at Göttingen, Germany.

Synthesis of Cp*$_2$(Me)Zr(μ-O)Ti(NMe$_2$)$_3$ (7). A solution of Cp*$_2$(Me)Zr(OH) (0.394 g, 1.00 mmol) in toluene (20 mL) was added drop-by-drop over a period of 15 min to a solution of Ti(NMe$_2$)$_4$ (0.224 g, 1.00 mmol) in toluene (30 mL) at 25 °C. The solution was then stirred at 25 °C for 24 h. The resulting light-yellow solution was then passed through an activated celite pad, concentrated to approximately 15 mL under reduced pressure, and kept at −20 °C for a day, yielding yellow microcrystals of analytical purity. Yield 0.520 g (91%). Mp 171−172 °C. ^{1}H NMR (500 MHz, C_6D_6, 25 °C, TMS): δ: 0.01 (s, 3H, Zr−CH_3); 1.89 (s, 30H, Zr−C$_5$(CH_3)$_5$); 3.14 (s, 18H, Ti−N(CH_3)$_2$). ^{13}C NMR (125.75 MHz, C_6D_6, 25 °C, TMS): δ: 11.3 (s, Zr−C$_5$(*C*H$_3$)$_5$); 29.1 (s, Zr−*C*H$_3$); 45.4 (s, Ti−N(*C*H$_3$)$_2$); 117.7 (s, Zr−*C*$_5$(CH$_3$)$_5$). MS (EI): *m*/*e* (relative intensity in %): 556.2 (14) [*M* − Me]$^+$; 526.2 (56) [*M* − NMe$_2$]$^+$; 511.1 (100) [*M* − Me and NMe$_2$]$^+$. Anal. Calcd for $C_{27}H_{51}N_3OTiZr$: C, 56.61; H, 8.97; N, 7.33. Found: C, 56.46; H, 8.65; N, 7.17.

Synthesis of Cp*$_2$(Me)Zr(μ-O)Hf(NMe$_2$)$_3$ (8). A solution of Cp*$_2$(Me)Zr(OH) (0.394 g, 1.00 mmol) in toluene (20 mL) was added drop-by-drop over a period of 15 min to a solution of Hf(NMe$_2$)$_4$ (0.354 g, 1.00 mmol) in toluene (30 mL) at −30 °C. The resulting solution was slowly warmed to ambient temperature. This solution was then stirred at 25 °C for 24 h. The title compound could not be isolated in a pure form. ^{1}H NMR spectroscopy of the reaction mixture showed formation of the title compound as the major product along with trimetallic **9** as the minor product. The ^{1}H NMR data for **8**: ^{1}H NMR (300 MHz, C_6D_6, 25 °C, TMS): δ: −0.07 (s, 3H, Zr−CH_3); 1.88 (s, 30H, Zr−C$_5$(CH_3)$_5$); 3.00 (s, 18H, Hf−N(CH_3)$_2$).

Synthesis of Cp*$_2$(Me)Zr(μ-O)Hf(NMe$_2$)$_2$(μ-O)Zr(Me)Cp*$_2$ (9). A solution of Cp*$_2$(Me)Zr(OH) (0.433 g, 1.1 mmol) in toluene (20 mL) was added drop-by-drop over a period of 15 min to a solution of Hf(NMe$_2$)$_4$ (0.177 g, 0.50 mmol) in toluene (20 mL) at −30 °C. The solution was slowly warmed to ambient temperature and was stirred at 25 °C for 24 h. The resulting solution was filtered, concentrated to approximately 15 mL under reduced pressure, and kept at −20 °C for several days, yielding colorless crystals of analytical purity. Yield 0.42 g (80%). Mp 312−313 °C. ^{1}H NMR (500 MHz, C_6D_6, 25 °C, TMS): δ: −0.05 (s, 6H, Zr−CH_3); 1.92 (s, 60H, Zr−C$_5$(CH_3)$_5$); 2.99 (s, 12H, Hf−N(CH_3)$_2$). ^{13}C NMR (125.75 MHz, C_6D_6, 25 °C, TMS): δ: 11.6 (s, Zr−C$_5$(*C*H$_3$)$_5$); 27.9 (s, Zr−*C*H$_3$); 43.5 (s, Hf−N(*C*H$_3$)$_2$); 117.7 (s, Zr−*C*$_5$(CH$_3$)$_5$). MS (EI): *m*/*e* (relative intensity in %): 1037.4 (24) [*M* − Me]$^+$, 1007.4 (32) [*M* − NMe$_2$]$^+$, 992.3 (100) [*M* − Me and NMe$_2$]$^+$. Anal. Calcd for $C_{46}H_{78}HfN_2O_2Zr_2$: C, 52.51; H, 7.47; N, 2.66. Found: C, 51.95; H, 7.29; N, 2.53.

X-ray Structure Determination of 7 and 9. Crystal data is presented in Table 1. The data was collected from shock-cooled crystals[33] at 100(2) K on a Bruker SMART-APEX II diffractometer with a D8 goniometer (graphite-monochromated Mo Kα radiation, λ = 0.71073 Å) equipped with a low-temperature device. The data was integrated with *SAINT*,[34] and an empirical absorption (*SADABS*) was applied.[35] The structures were solved by direct methods (*SHELXS-97*)[36] and refined by full-matrix least-squares methods against F^2 (*SHELXL-97*).[37] All of the non-hydrogen atoms were refined with anisotropic displacement parameters. The hydrogen atoms were refined isotropically on calculated positions using a riding model with their U_{iso} values constrained to equal to 1.5 times

(33) Stalke, D. *Chem. Soc. Rev.* **1998**, *27*, 171−178.
(34) *SAINT-NT*; Bruker-AXS Inc.: Madison, WI, U.S.A., 2000.
(35) Sheldrick, G. M. *SADABS 2.0*; University of Göttingen: Göttingen, Germany, 2000.
(36) Sheldrick, G. M. *Acta Crystallogr., Sect. A* **1990**, *46*, 467−473.
(37) Sheldrick, G. M. *SHELXL-97*; University of Göttingen: Göttingen, Germany, 1997.

the U_{eq} of their parent carbon atom. Crystallographic data (excluding structure factors) have been deposited with the Cambridge Crystallographic Data Centre (CCDC numbers see Table 1). Copies of the data can be obtained free of charge from the CCDC via www.ccdc.cam.ac.uk/data_request/cif.

Computational Details. The calculations were performed at the well-established DFT level of theory making use of the B3LYP functional[38,39] as implemented in the *Gaussian* program package[40] employing a basis-set termed LANL2DZ[41] for titanium and 6-31G[42,43] for the remaining atoms. In the first step, the compound was fully optimized to its equilibrium structure. The resulting electronic wave function for the structure was then analyzed to obtain the shape of the molecular orbitals and a NBO analysis[44−46] was performed to ascertain the bonding situation. The ab initio calculations were performed on the probable cationic species centered on zirconium and on titanium, which are supposed intermediates in the polymerization process.

(38) Lee, C.; Yang, W.; Parr, R. G. *Phys. Rev. B* **1988**, *37*, 785−789.
(39) Miehlich, B.; Savin, A.; Stoll, H.; Preuss, H. *Chem. Phys. Lett.* **1989**, *157*, 200−206.
(40) Frisch, M. J.; Trucks, G. W.; Schlegel, H. B.; Scuseria, G. E.; Robb, M. A.; Cheeseman, J. R.; Montgomery, J. A., Jr.; Vreven, T.; Kudin, K. N.; Burant, J. C.; Millam, J. M.; Iyengar, S. S.; Tomasi, J.; Barone, V.; Mennucci, B.; Cossi, M.; Scalmani, G.; Rega, N.; Petersson, G. A.; Nakatsuji, H.; Hada, M.; Ehara, M.; Toyota, K.; Fukuda, R.; Hasegawa, J.; Ishida, M.; Nakajima, T.; Honda, Y.; Kitao, O.; Nakai, H.; Klene, M.; Li, X.; Knox, J. E.; Hratchian, H. P.; Cross, J. B.; Bakken, V.; Adamo, C.; Jaramillo, J.; Gomperts, R.; Stratmann, R. E.; Yazyev, O.; Austin, A. J.; Cammi, R.; Pomelli, C.; Ochterski, J. W.; Ayala, P. Y.; Morokuma, K.; Voth, G. A.; Salvador, P.; Dannenberg, J. J.; Zakrzewski, V. G.; Dapprich, S.; Daniels, A. D.; Strain, M. C.; Farkas, O.; Malick, D. K.; Rabuck, A. D.; Raghavachari, K.; Foresman, J. B.; Ortiz, J. V.; Cui, Q.; Baboul, A. G.; Clifford, S.; Cioslowski, J.; Stefanov, B. B.; Liu, G.; Liashenko, A.; Piskorz, P.; Komaromi, I.; Martin, R. L.; Fox, D. J.; Keith, T.; Al-Laham, M. A.; Peng, C. Y.; Nanayakkara, A.; Challacombe, M.; Gill, P. M. W.; Johnson, B.; Chen, W.; Wong, M. W.; Gonzalez, C.; Pople, J. A. *Gaussian 03*, revision C.02; Gaussian, Inc.: Wallingford, CT, 2004.
(41) Hay, P. J.; Wadt, W. R. *J. Chem. Phys.* **1985**, *82*, 270−283.
(42) Petersen, G. A.; Al-Laham, M. A. *J. Chem. Phys.* **1991**, *94*, 6081−6090.
(43) Petersen, G. A.; Bennett, A.; Tensfeldt, T. G.; Al-Laham, M. A.; Shirley, W. A.; Mantzaris, J. *J. Chem. Phys.* **1988**, *89*, 2193−2218.
(44) Foster, J. P.; Weinhold, F. *J. Am. Chem. Soc.* **1980**, *102*, 7211−7218.
(45) Reed, A. E.; Weinhold, F. *J. Chem. Phys.* **1985**, *83*, 1736−1740.
(46) Reed, A. E.; Curtiss, L. A.; Weinhold, F. *Chem. Rev.* **1988**, *88*, 899−926.

Polymerization of Ethylene and Styrene. The polymerization reactions were carried out on a vacuum line (10^{-5} Torr) in an autoclave (Buchi). In a typical experiment, 100 mL of dry toluene (from Na/K) was vacuum-transferred into the polymerization flask and saturated with 1.0 atm of rigorously purified ethylene (for ethylene polymerization) or with argon in the presence of 10 mL of dry styrene (from CaH_2) (for styrene polymerization). The catalyst (10 μmol) was taken in the Schlenk flask and the appropriate MAO (1.6 M in toluene, Witco GmbH) was added. The mixture was stirred for 20 min to activate the catalyst. The catalyst solution was then quickly injected into the rapidly stirred flask using a gastight syringe. After a measured time interval, the polymerization was quenched by the addition of 5 mL methanol, and the reaction mixture was then poured into 800 mL methanol. The polymer was allowed to fully precipitate overnight and then was collected by filtration, washed with fresh methanol, and dried. The results are shown in Tables 3 and 4.

Polymer Characterization. ^{13}C NMR assays of polymer microstructure were conducted in 1,1,2,2-tetrachloroethane-d_2 at 110 °C. The polymer melting range was measured on a TA instrument 2920 (modulated differential scanning calorimeter), which was calibrated against indium metal. The measurements were carried out with a heating rate of 10 °C/min, using typically ca. 4 mg samples. Gel permeation chromatography was carried out at Basell R & D Polymer Physics and Characterization, Industriepark, Hoechst, Frankfurt (Germany). 1,2,4-Trichlorobenzene was used as solvent. The columns were calibrated with narrow molecular weight distribution standards of polystyrene.

Acknowledgment. This work is supported by the Göttinger Akademie der Wissenschaften, Deutsche Forschungsgemeinschaft, and the Fonds der Chemischen Industrie. S.K.M. thanks the Alexander von Humboldt Foundation for a research fellowship.

Supporting Information Available: X-ray data of **7** and **8** (CIF), space filling models of **7** and **9**, additional table containing polymerization results, and calculated atomic coordinates of **7** (PDF). This material is available free of charge via the Internet at http://pubs.acs.org.

IC7011765